BROOKHAVEN NATIONAL LABORATORY

June 1991 BNL-46382

ISOSPIN MIXING IN PROTONIUM AND ANNIHILATION DYNAMICS

C. B. Dover

Department of Physics
Brookhaven National Laboratory, Upton, NY 11973

and

J.-M. Richard[1,2] and J. Carbonell[2]

[1] CERN, Theory Division
CH–1211 Geneva 23, Switzerland
and

[2]Institut des Sciences Nucléaires
Université Joseph–Fourier – CNRS – IN2P3
53, Avenue des Martyrs, F–38026 Grenoble Cedex, France

ABSTRACT

We have explored the sensitivity of $p\bar{p} - n\bar{n}$ isospin mixing in $L = 0, 1$ atomic states of protonium to changes in the multi–pion exchange contribution to the nucleon–antinucleon ($N\overline{N}$) potential. The resulting annihilation probabilities γ_I^α for isospin $I = 0, 1$ and state $\alpha = {}^{2S+1}\mathrm{L}_J$ are combined with the spin–flavor weights for transitions $N\overline{N} \to M_1 M_2$ in the ${}^3\mathrm{P}_0$ model, and confronted with selected measured branching ratios. Some problems with the phenomenology of the ${}^3\mathrm{P}_0$ model are identified. We compare the ${}^3\mathrm{P}_0$ model with a phenomenological ansatz suggested by Klempt, in which branching ratios are written as a product of spin, isospin and orbital factors, multiplied by γ_I^α.

1. Introduction

It has often been stressed, for example by Shapiro[1], that the nucleon–antinucleon ($N\overline{N}$) interaction results from a subtle interplay between long–range meson exchange forces and short–range absorption. The large value of the annihilation cross section, for instance, is due to the long–range attraction which focuses the wave–function towards the annihilation region[1].

A more refined analysis shows that the medium and long–range forces, though attractive on the average, exhibit a strong spin and isospin dependence. In some partial waves, the potential is strongly attractive while it is repulsive in other channels[2,3]. We thus expect annihilation to be substantially enhanced or suppressed in some initial states.

Protonium is the corner stone of this physics. Most data correspond to $N\overline{N}$ annihilation at rest, i.e. from protonium levels of orbital angular momentum $L = 0, 1$. Model calculations have shown that the distortion of the $N\overline{N}$ wave function is dramatically spin and isospin dependent in the case of protonium[4–7].

The aim of the present paper is twofold. First, we return to the calculation of the protonium wave function in optical models and analyze how it is sensitive to the details of the input model. In particular, we wish to compare models which contain only the one–pion–exchange tail in addition to absorption with models where two–pion–exchange effects (in particular ρ–meson exchange) are included. Secondly, we discuss the influence of the spin–isospin dependence of the protonium wave function on the phenomenology of branching ratios. This subject has received considerable attention in recent years[8–11]. It is still an open question whether annihilation diagrams with planar or rearrangement topology dominate, or whether there is any simple rule at all determining annihilation at the quark level.

2. Initial State Interaction

The spin and isospin structure of the $N\overline{N}$ potential has been analyzed at length in Refs. (2, 3). The dominant feature is the strong tensor component in the isospin $I = 0$ potential, arising from the coherent contributions of π, ρ and ω exchanges. This results in a strong repulsion in the $S = 1$, $J = L$ partial waves, for example $^{13}P_1$. In contrast,

in natural parity states there is a strong mixing of the $^{2I+1,2S+1}L_J$ components $^{13}(J-1)_J$ and $^{13}(J+1)_J$, resulting in a strong attraction for the appropriate combination of the two partial waves[3].

The consequences of spin–isospin structure for protonium have been discussed in Refs. (4-7). First, the $^1S_0$ and $^3S_1$ levels receive different energy shifts. The same is true for the four possible $^{2S+1}L_J$ levels for $L = 1$. It has not yet been possible to measure these fine structure effects. Secondly, the corresponding widths are also different. For instance, in a typical calculation[6] of the $2P$ level, $\Gamma(^3P_0) \simeq 110$ meV, while $\Gamma(^1P_1) \simeq 20$ meV. Finally, the neutron–antineutron ($n\bar{n}$) admixture in the protonium wave function is a quite important effect at short distances $r \lesssim 1$ fm. It does not significantly increase the total hadronic width, except perhaps for the $^3P_0$ state, but it dramatically affects the sharing of this width between the $I = 0$ and the $I = 1$ components[6,7]. In Ref. 7 a comparison is shown of the values obtained from the Dover–Richard[6,12](DR1 and DR2) and Kohno–Weise[13](KW) potentials: the differences are small. Furui *et al.*[14] have considered a wider class of models with somewhat larger differences. In Table 1, we present the results of a calculation with the pion exchange only in the external part and the same cut–off procedure and annihilation core as in DR2. More precisely, we consider a model

$$V = V_{\rm ann} + V_\pi + xV_{2\pi+\omega} \tag{1}$$

where $x = 1$ corresponds to the original DR2 model[6] and, for $x = 0$, only the pion tail is left. The quantities of interest are Γ, the total annihilation width and $y = \Gamma_1/\Gamma_0$ which measures the sharing of annihilation between the $I = 1$ and $I = 0$ components. Remember that $y = 1$ would be automatic if the charge–exchange potential, which couples the $p\bar{p}$ and $n\bar{n}$ channels, is neglected. Note that we do not introduce explicitly the coupling to other baryon–antibaryon configurations, such as $N\overline{\Delta}$, $\Delta\overline{N}$, $\Delta\overline{\Delta}$, etc., which could significantly contribute to annihilation at short distances.

The first surprise in Table 1 is that ΔE, Γ and y depend very little on x. This deserves some explanation. Consider for instance the $^3P_0$ state. For $x = 0$, the potential is attractive in $I = 0$, repulsive in $I = 1$. Thus the radial wave function $u(^{33}P_0)$ is suppressed while $u(^{13}P_0)$ is enhanced at short distances and even starts exhibiting oscillations. With a purely real potential and in a one–channel situation $u(^{13}P_0)$ would have a node, since the

atomic state is a radial excitation of a nuclear bound state; these oscillations are damped by absorption and isospin mixing. Now, when ρ–meson exchange and other intermediate range forces are switched on, $u(^{33}P_0)$ is not suppressed too much further: we are in a regime where the wave function varies non–linearly as a function of the potential strength. On the other hand, the oscillations of $u(^{13}P_0)$ become more pronounced as x increases, but this does not change its width very much. This is illustrated in Figs. 1 and 2 where we display the annihilation densities $d(r)$ of $^{13}P_0$ and $^{33}P_0$ wave function components for $x = 0$ and $x = 1$, defined as

$$\Gamma = \int_0^\infty d(r)\, dr \qquad d(r) = -2|u|^2\, \mathrm{Im}\,(V) \tag{2}$$

The stability of the width ratio y with respect to x is somewhat frustrating, if our goal is to draw some conclusions regarding the role of intermediate range forces in protonium. On the other hand, it implies that our predictions for the channel dependence of the Γ's are not very model dependent and thus more stable than one may have anticipated. In fact, the x dependence of the protonium wave function is more pronounced in the $p\bar{p}$-$n\bar{n}$ basis and it is partially cancelled out when one reconstructs the isospin states relevant for calculating annihilation branching ratios. Also, the stability with respect to x is less pronounced for models without a strong real part in the annihilation potential, such as Ref. 13.

3. Testing Annihilation Mechanisms

For a given initial state the observed branching ratios into two mesons also depend on the relative strengths of the various $N\bar{N} \to M_1 M_2$ transitions. The experiments at the Low Energy Antiproton Ring (LEAR) facility at CERN[15] have motivated a resurgence of interest in theoretical models of the annihilation process. Statistical models, models assuming factorization of spin and flavor amplitudes, dominance of rearrangement diagrams with minimal change of the initial quark content, dominance of annihilation diagrams with planar topology, etc., have all led to different predictions[8]. To test these models, one would like to separate the effects of initial state interactions from the intrinsic annihilation rates.

A first idea consists of comparing channels with the same quantum numbers. For instance, $\pi^0\pi^0$ and $\eta\eta$ arise from the same $^{13}P_0$ and $^{13}P_2$ channels. However, these two

decays involve quite different momentum transfers q, and hence are sensitive to different regions of the same $N\overline{N}$ radial wave functions $u(r)$. Since $u(r)$ is likely to exhibit a node, or, at least, sharp variations[7,16](see Fig. 1), the ratio $\pi\pi/\eta\eta$ cannot be reduced to a simple product of phase–space and Clebsch–Gordan factors.

Another strategy was recently attempted by Klempt[17], who compared two–meson channels with about the same q value, but different isospin. An example is the ratio $\eta\omega/\eta\rho$. Adopting this strategy, we extend somewhat the results of Klempt[17] to predict a number of other ratios of two–body modes. These are compared to the predictions of a modified version of the $^3P_0$ model[9], in which the effects of $p\bar{p} - n\bar{n}$ mixing are included as isospin probabilities, as in the model of Klempt[17]. In a number of cases, particularly for $L = 1$, these two models yield ratios which differ by an order of magnitude. We argue that a systematic measurement of such two–body branching ratios B for both $L = 0, 1$ will allow one to clearly distinguish between these two models. In view of the extreme simplicity of this treatment of initial state interactions, we would not be surprised if more comprehensive and precise data led to the demise of both models.

4. Two Simple Models

In the approach of Klempt[17], the branching ratio B for a transition from an $N\overline{N}$ atomic state $i = \{LSJ\}$ to a two meson final state $M_1 + M_2$ (isospins I_1, I_2) is written as[19,20]

$$B^i(M_1, M_2) = (2J+1)\, C(I; I_1 I_2)\, f(1,2)\, \gamma_I(i)\, /\Gamma_{\rm tot}(i) \qquad (3)$$

Here, $\gamma_I(i)$ is the probability that the state i has isospin I, with normalization condition $\gamma_0^i + \gamma_1^i = 1$. The allowed value of I is determined by G–parity conservation: $(-)^{L+S+I} = G_1 G_2$, where G_i are the G–parities of the mesons. The total width of state i is given by $\Gamma_{\rm tot}(i)$. For a pure $p\bar{p}$ initial state, we have $\gamma_0(i) = \gamma_1(i) = 1/2$. When $p\bar{p} - n\bar{n}$ mixing is included, we identify $\gamma_1(i)/\gamma_0(i)$ with the rate $y = \Gamma_1/\Gamma_0$ of total annihilation widths for state i, as shown in Table 1. For our numerical estimates, we adopt the isospin probabilities shown in Table 2. In Eq. (3), $f(1,2)$ is the kinematical form factor; in Ref. 17, it is assumed to depend on q and the relative orbital angular momentum ℓ of the $M_1 M_2$ system. In the $^3P_0$ model[9], $f(1,2)$ also depends on the $N\overline{N}$ orbital angular momentum

L. Since we only form ratios of rates for transitions with the same $\{L, \ell\}$ values and approximately the same q, $f(1,2)$ cancels out, and we do not need to specify its form here. Finally, $C(I; I_1 I_2)$ is a phenomenological factor, assumed to depend only on isospin, and determined by Klempt[17] via a fit to certain branching ratios for $L = 0$. For instance, we have[21], assuming $\Gamma_{\rm tot}(^1{\rm S}_0) = \Gamma_{\rm tot}(^3{\rm S}_1)$, the ratios

$$C\,(1;01)\,/C\,(0;00) = \frac{\gamma_0^t}{\gamma_1^t}\,\frac{B^t\,(\eta\rho^0)}{B^t\,(\eta\omega)} \approx \frac{1}{2} \tag{4a}$$

$$C\,(0;11)\,/C\,(0;00) = \frac{B^t\,(\eta\rho^0)\,B^t\,(\pi^0\rho)}{B^t\,(\eta\omega)\,B^t\,(\pi^0\omega)} \approx \frac{3}{4} \tag{4b}$$

$$C\,(1;11)\,/C\,(0;00) = \frac{\gamma_0^s}{3\gamma_1^t}\cdot\frac{B^t\,(\pi^+a_2^-)}{B^s\,(\pi^+a_2^-)}\cdot\frac{C\,(0;11)}{C\,(0;00)} \approx \frac{1}{10} \tag{4c}$$

where the superscripts t and s refer to $^3{\rm S}_1$–$^3{\rm D}_1$ and $^1{\rm S}_0$ initial $N\overline{N}$ states, respectively. The numerical values in Eqs. (4a–c) result from using the $\gamma_I(i)$ values in Table 2 and the measured ratios[17]

$$\frac{B^t\,(\pi^0\omega)}{B^t\,(\pi^0\rho)} = 0.57^{+0.09}_{-0.15} \tag{5a}$$

$$\frac{B^t\,(\eta\rho^0)}{B^t\,(\eta\omega)} = 0.42 \pm 0.05 \tag{5b}$$

$$\frac{B^t\,(\pi^+a_2^-)}{B^s\,(\pi^+a_2^-)} = 0.34 \pm 0.07 \tag{5c}$$

Note that the ratios of C's are very different from the ratios of isospin Clebsch–Gordon coefficients, which would correspond to 1, 1/3, 1/2 for Eqs. (4a–c), respectively; this latter assumption is made by Vandermeulen[22].

The second model we consider is a variant of the $^3{\rm P}_0$ model[23,9], in which we write

$$B^i\,(M_1, M_2) = (2J+1)\cdot SF\,(i \to M_1 M_2)\; f\,(1,2)\;\gamma_I\,(i)\,/\Gamma_{\rm tot}\,(i) \tag{6}$$

where $SF(i \to M_1 M_2)$ are the spin–flavor weights tabulated by Maruyama *et al.*[9]. These weights, unlike $C(I; I_1 I_2)$, depend on $\{LSJ\ell\}$, so there is no factorization of spin and isospin terms. The values of SF are calculated from the planar diagram shown in Fig. 3 (sometimes referred to as "A2" in the literature), where two quark–antiquark ($Q\overline{Q}$) pairs

are annihilated and one created, each vertex being described in the $^3P_0$ model in terms of $Q\overline{Q}$ pairs with vacuum quantum numbers $(0^{++}(0^+))$.

In Eq. (6), as well as Eq. (3), the full effect of initial state interactions is subsumed in the isospin probability $\gamma_I(i)$, and final state meson–meson interactions are ignored. This represents a drastic simplification of the complicated dynamics of the $N\overline{N}$ annihilation problem. Nevertheless, it is of interest to work out the detailed predictions of these two models, which differ qualitatively in certain cases and are very similar in others.

5. Consequences for S–wave Annihilation

In the $^3P_0$ model, we obtain the equality

$$\frac{B^t(\pi^0\omega)}{B^t(\pi^0\rho^0)} = \frac{B^t(\eta\rho^0)}{B^t(\eta\omega)} = \frac{B^t(\rho f_2)}{B^t(\omega f_2)} = \frac{B^t(\eta_{id}\rho^0)}{B^t(\pi^0\rho^0)} = \frac{3}{4}\frac{\gamma_1^t}{\gamma_0^t} \tag{7}$$

where $\eta_{id} = (u\bar{u} + d\bar{d})/\sqrt{2}$ corresponds to ideal mixing. For a pseudoscalar mixing angle $\theta_{PS} \simeq -20°$, as in Ref. 18, we have

$$B(\eta X) \approx \frac{2}{3}B(\eta_{id}X) \tag{8}$$

The equality (7) is consistent with Eqs. (5a,5b) and the measured ratios[17]

$$\frac{B^t(\rho^0 f_2)}{B^t(\omega f_2)} = 0.48 \pm 0.12, \quad \frac{B^t(\eta\rho^0)}{B^t(\pi^0\rho^0)} = 0.28 \pm 0.03 \tag{9}$$

if we choose

$$\frac{\gamma_1^t}{\gamma_0^t} \approx 0.63 \pm 0.07 \tag{10}$$

This is close to the ratio $y = 0.8$ shown in Table 1 for the $^3S_1$–$^3D_1$ state, which includes the strong effects of tensor coupling. The equality of the ratios (7) can also be understood in the model on Eq. (3) if a somewhat larger value $\gamma_1^t/\gamma_0^t = 1.17^{+0.39}_{-0.28}$ is chosen[17]. A characteristic of model calculations which include tensor coupling is that $\gamma_1^t/\gamma_0^t < 1$, so that Eq. (10) seems more consistent with theoretical expectations.

With the C's of Eq. (3) now determined, one can make a number of consistency checks involving other ratios. For instance, we predict

$$\frac{B^s(\pi^+\rho^-)}{B^t(\pi^+\rho^-)} = \frac{\gamma_0^s\gamma_1^s}{9\gamma_0^t\gamma_1^t} \cdot \frac{B^t(\pi^+a_2^-)}{B^s(\pi^+a_2^-)} \tag{11}$$

Using the values $B^s(\pi^+\rho^-) = (4.6 \pm 2.0) \times 10^{-4}$ and $B^t(\pi^+\rho^-) = (165 \pm 8) \times 10^{-4}$ from Ref. 17, we obtain

$$B^s\left(\pi^+\rho^-\right)/B^t\left(\pi^+\rho^-\right) = 2.8 \pm 1.4 \times 10^{-2} \tag{12}$$

The smallness of this ratio is known as the "$\pi\rho$ puzzle", and represents an example of an approximate dynamical selection rule in $N\overline{N}$ annihilation. Using the πa_2 ratio of Eq. (5c), we find that Eq. (11) is approximately satisfied. In the model of Eq. (3), this dynamical selection rule is a consequence of the smallness of the ratio $C(1;11)/C(0;00)$, as per Eq. (4c). Note that this is the result of a fit, and is not a dynamical prediction. If we assume the C ratios are independent of L, as in Ref. 17, we also predict dynamical selection rules for $L = 1$; the non–appearance of these would rule out the model of Eq. (3). The $L = 1$ case is treated in the next section.

In the $^3\mathrm{P}_0$ model of Eq. (6), we predict

$$\frac{B^t\left(\pi^+a_2^-\right)}{B^s\left(\pi^+a_2^-\right)} = \frac{3\gamma_1^t}{\gamma_0^s}\left(\frac{18.778}{18}\right) \approx 2.5 \tag{13}$$

including only the contribution $^{33}\mathrm{S}_1 \to \pi^+a_2^-(\ell = 2)$ in the numerator. The factor in brackets arises from the SF weights. This disagrees qualitatively with Eq. (5c). Similarly, including only $^{13}\mathrm{S}_1$, we would obtain

$$\frac{B^s\left(\pi^+\rho^-\right)}{B^t\left(\pi^+\rho^-\right)} = \frac{\gamma_1^s}{3\gamma_0^t}\left(\frac{3}{2}\right) \approx 0.4 \tag{14}$$

in disagreement with Eq. (12). Thus the simple form (6) of the $^3\mathrm{P}_0$ model fails to reproduce the $\pi\rho$ or πa_2 dynamical selection rules. For the $\pi\rho$ case, it has been shown by Maruyama *et al.*[10], that *constructive interference* of $^{13}\mathrm{S}_1$ and $^{13}\mathrm{D}_1$ initial states, neglected in Eq. (14), is crucial in understanding the "$\pi\rho$ puzzle". Such interference phenomena cannot be understood in terms of isospin probabilities alone, as postulated in Eq. (6). Each case must be treated separately, since the interference will depend on ℓ and q. For instance, a large *destructive* $^{33}\mathrm{S}_1 - {}^{33}\mathrm{D}_1 \to \pi a_2(\ell = 2)$ interference is needed to bring Eq. (13) in accord with Eq. (5c). However, the tensor mixing[3] is much less significant for $I = 1$ than for $I = 0$, so the interference is expected to less dramatic than for $\pi\rho$. It would be worthwhile to systematically investigate such interferences in mesonic channels fed by the $^{13}\mathrm{S}_1$–$^{13}\mathrm{D}_1$ initial state; in addition to $\pi\rho(\ell = 1)$, these include $\eta\omega(\ell = 1)$ and $\pi b_1(\ell = 0, 2)$.

For $L = 0$, there are several other ratios which involve the same $\{L\,\ell\,q\}$ values. These are collected in Table 3. The experimental data have large error bars and are somewhat contradictory. We have

$$B^s\left(\rho^0\omega\right) = \begin{cases} 22.6 \pm 2.3 \times 10^{-3} & \text{Bizzarri } et\ al.^{24} \\ 7 \pm 3 \times 10^{-3} & \text{Baltay } et\ al.^{25} \end{cases} \qquad (15a)$$

$$B^s\left(\omega\omega\right) = 14 \pm 6 \times 10^{-3} \qquad \text{Bloch } et\ al.^{26} \qquad (15b)$$

$$B^s\left(\rho^0\rho^0\right) = \begin{cases} 1.2 \pm 1.2 \times 10^{-3} & \text{Diaz } et\ al.^{27} \\ 4 \pm 3 \times 10^{-3} & \text{Baltay } et\ al.^{28} \end{cases} \qquad (15c)$$

from which we obtain the ratios

$$B^s\left(\rho^0\rho^0\right)/B^s\left(\omega\omega\right) = \begin{cases} 0.09^{+0.21}_{-0.09} & \text{Diaz } et\ al.^{27} \\ 0.29^{+0.59}_{-0.24} & \text{Baltay } et\ al.^{28} \end{cases} \qquad (16a)$$

$$B^s\left(\rho^0\omega\right)/B^s\left(\omega\omega\right) = \begin{cases} 1.6^{+1.3}_{-0.6} & \text{Bizzarri } et\ al.^{24} \\ 0.5^{+0.8}_{-0.3} & \text{Baltay } et\ al.^{25} \end{cases} \qquad (16b)$$

Using the values $B^s(\pi^0 a_2^0) = (132 \pm 31) \times 10^{-4}$ and $B^s(\pi^0 f_2) = 39.6 \pm 7.9 \times 10^{-4}$ given by Klempt[17], we find

$$B^s\left(\pi^0 a_2^0\right)/B^s\left(\pi^0 f_2\right) = 3.3^{+1.8}_{-1.2} \qquad (17)$$

Comparing Eqs. (16) and (17) with the predictions of Table 3, we see that the $^3P_0$ model does not seem to be consistent with any of the above ratios, although we must emphasize that the error bars are very large. Unfortunately, new results from LEAR experiments on $\rho\rho$, $\rho\omega$ and $\omega\omega$ modes have not yet been published. The Klempt model may be consistent with the $\pi a_2/\pi f_2$ and $\rho^0\omega/\omega\omega$ ratios, but provides no mechanism for the apparent suppression of $\rho^0\rho^0/\omega\omega$. Precise experimental data are needed to test these simple models more stringently.

6. Consequences for P–wave Annihilation

Our two models differ rather dramatically in their dependence on the initial state orbital angular momentum L. Klempt[17] assumes that the C's in Eq. (3) are independent of L. There is no motivation for this assumption except simplicity, but it is worth testing in any case. In the $^3P_0$ model, on the other hand, the factors SF of Eq. (6) depend strongly on L for a fixed transition $N\overline{N} \to M_1 M_2$. We now compare transitions with approximately the same q, as before, and point up the qualitative differences between the two models.

First consider the $L = 1$ ratios analogous to Eq. (7). We find

$$\frac{B\left(^1P_1 \to \pi^0\omega\right)}{B\left(^1P_1 \to \pi^0\rho\right)} = \frac{B\left(^1P_1 \to \eta\rho^0\right)}{B\left(^1P_1 \to \eta\omega\right)} = \frac{B\left(^1P_1 \to \rho^0 f_2\right)}{B\left(^1P_1 \to \omega f_2\right)} = \frac{B\left(^1P_1 \to \eta_{id}\rho^0\right)}{B\left(^1P_1 \to \pi^0\rho^0\right)} \tag{18}$$

$$= \begin{cases} \dfrac{C\left(1;01\right)\gamma_1\left(^1P_1\right)}{C\left(0;11\right)\gamma_0\left(^1P_1\right)} \approx 0.46 & \text{[Eq. (3)]} \\ 2.78\gamma_1\left(^1P_1\right)/\gamma_0\left(^1P_1\right) \approx 1.7 & \text{[Eq. (6)]} \end{cases}$$

These ratios, which are not yet experimentally determined, are seen to be significantly different for the two models: this is due to the marked increase in the SF ratio from 3/4 for $L = 0$ to 2.78 for $L = 1$ in the $^3P_0$ model.

The predicted ratios for p–wave annihilation which are analogous to those shown in Table 3, are displayed in Table 4. When several initial J values contribute, we add the contributions with the statistical weight $(2J + 1)$. For example, we write

$$\frac{B\left(^3P_{0,1,2} \to \pi^0 a_1^0\left(\ell = 1\right)\right)}{B\left(^3P_{0,1,2} \to \pi^0 f_1\left(\ell = 1\right)\right)} = \frac{\left[\tilde{\gamma}_0\left(^3P_0\right) + 3\tilde{\gamma}_0\left(^3P_1\right) + 5\tilde{\gamma}_0\left(^3P_2\right)\right]}{\left[\tilde{\gamma}_1\left(^3P_0\right) + 3\tilde{\gamma}_1\left(^3P_1\right) + 5\tilde{\gamma}_1\left(^3P_2\right)\right]} \cdot \frac{C\left(0;11\right)}{C\left(1;01\right)} \tag{19}$$

from Eq. (3), where $a_1 = a_1(1260)[1^{++}(1^-)]$ and $f_1 = f_1(1285)[1^{++}(0^+)]$. Here, we define $\tilde{\gamma}_I(i) = \frac{\gamma_I(i)}{\Gamma_{\rm tot}(i)}$. If two different ℓ values occur, the corresponding ratios are generally different for the $^3P_0$ model, so we quote them separately (for $L = 0$, the $\ell = 0$ and $\ell = 2$ ratios discussed previously are the same).

In Table 4, we note that the only significant difference between the two models is in the $\pi^0 b_1^0/\pi^0 h_1$ ratio. In the $^3P_0$ model, the SF matrix elements for the transitions $^{11}P_1 \to \pi^0 b_1^0(\ell = 1)$ and $^{31}P_1 \to \pi^0 h_1(\ell = 1)$ both vanish. These are two examples of dynamical selection rules predicted by the $^3P_0$ model, i.e. transitions which are allowed

by conservation of $J^{\pi C}(I^G)$ quantum numbers, but in fact forbidden by the dynamics of the model. It will be very interesting to see if there is any sign of these $^3P_0$ selection rules in the $L = 1$ data from LEAR.

In Table 5, we display predicted ratios of charged to neutral modes for the same final state M_1M_2. In the Klempt model, each of these ratios is a product of $C(1;11)/C(0;11) \approx 2/15$ and a factor depending on isospin probabilities. The smallness of $C(1;11)/C(0;11)$ which successfully describes the small ratios (5c) and (12) for $L = 0$, then implies a number of approximate dynamical selection rules for $L = 1$ as indicated in Table 5. In the case of the ratios $\pi^+\rho^-/\pi^0\rho^0$ or $\pi^+a_2^-/\pi^0a_2^0$, the predictions of the $^3P_0$ model are of order unity, so the two models are clearly distinguished. If the suppressed ratios predicted by the Klempt model for $L = 1$ are not found in the data, the model can be rejected. Alternatively, one could argue that the C's could be independently fit to the $L = 1$ data, but such a model would have little content.

The annihilation process $N\bar{N}(L = 1) \to \pi\rho$ was studied in detail by the ASTERIX collaboration at LEAR (B. May *et al.*[29]). They give

$$\frac{B\left(^3P_1 \to \pi^+\rho^-\right)}{B\left(^1P_1 \to \pi^0\rho^0\right)} \approx 0.64 \tag{20}$$

which does not suggest a dynamical selection rule for the $L = 1$ $\pi\rho$ system. As seen from Table 5, neither the Klempt model nor the $^3P_0$ model is in agreement with Eq. (20). Another potential difficulty for the $^3P_0$ model is seen in the $\pi a_2/\pi f$ ratio. Klempt[17] gives

$$\begin{aligned} B\left(L = 1 \to \pi^+a_2^-\right) &= 4.5 \pm 2.4 \times 10^{-3} \\ B\left(^{33}P_1 \to \pi^0 f_2\right) &= 18.0 \pm 2.5 \times 10^{-3} \end{aligned} \tag{21}$$

and hence

$$\frac{B\left(L = 1 \to \pi^+a_2^-\right)}{B\left(^{33}P_1 \to \pi^0 f_2\right)} = 0.25^{+0.2}_{-0.15} \tag{22}$$

The allowed $L = 1$ transitions are $^{13}P_{1,2} \to \pi^+a_2^-$ and $^{13}P_1 \to \pi^+a_2^-$. Using the SF weights of Ref. 9 and isospin probabilities and widths from Table 2, we predict

$$\frac{B\left(L = 1 \to \pi^+a_2^-\right)}{B\left(^{33}P_1 \to \pi^0 f_2\right)} \approx 0.7, \tag{23}$$

larger than Eq. (22). Similarly, it is difficult to explain the observed smallness of this ratio using the model of Eq. (3). In this case, we predict

$$\frac{B\left(L=1\to\pi^+a_2^-\right)}{B\left(^{33}\mathrm{P}_1\to\pi^0f_2\right)}=\frac{\left[3\tilde{\gamma}_0\left(^3\mathrm{P}_1\right)C\left(0;11\right)+5\tilde{\gamma}_0\left(^3\mathrm{P}_2\right)C\left(0;11\right)+3\tilde{\gamma}_1\left(^1\mathrm{P}_1\right)C\left(1;11\right)\right]}{3\tilde{\gamma}_1\left(^3\mathrm{P}_1\right)C\left(1;01\right)}\approx 1.2 \tag{24}$$

The results (23) and (24) are rather sensitive to how we treat the coupled $^{13}\mathrm{P}_2$–$^{13}\mathrm{F}_2$ partial wave. In the above, we have attributed the entire probability γ_0 to the $^{13}\mathrm{P}_2$ component. In the tensor–coupled calculations[7], $\gamma_0 = 0.60$ in Table 2 splits up into 0.37 for the $^{13}\mathrm{P}_2$ component and 0.23 for $^{13}\mathrm{F}_2$. If we simply suppress the $^{13}\mathrm{F}_2$ piece, the ratios (23) and (24) become 0.56 and 0.85, respectively. Finally, if we make the extreme assumption of complete *destructive* interference of $^{13}\mathrm{P}_2 \to \pi a_2$ and $^{13}\mathrm{F}_2 \to \pi a_2$ amplitudes, we would obtain 0.35 and 0.28 for Eqs. (23) and (24), not far from the experimental value of Eq. (22). Clearly one should take such interferences into account explicitly, particularly for $I = 0$ channels.

One can also use the ratio (22) to obtain a limit on $\gamma_0(^3\mathrm{P}_1)/\gamma_1(^3\mathrm{P}_1)$, since we have

$$\frac{B\left(L=1\to\pi^+a_2^-\right)}{B\left(^{33}\mathrm{P}_1\to\pi^0f_2\right)}>\xi\frac{\gamma_0\left(^3\mathrm{P}_1\right)}{\gamma_1\left(^3\mathrm{P}_1\right)} \tag{25}$$

where

$$\xi = C\left(0;11\right)/C\left(1;01\right)\approx 3/2$$

for the Klempt model and

$$\xi = SF\left(^{13}\mathrm{P}_1\to\pi^+a_2^-\right)/SF\left(^{33}\mathrm{P}_1\to\pi^0f_2\right)=1/3$$

for the $^3\mathrm{P}_0$ model. From Eq. (22), we then obtain

$$\frac{\gamma_1\left(^3\mathrm{P}_1\right)}{\gamma_0\left(^3\mathrm{P}_1\right)}>\begin{cases}6 & \text{(Klempt)}\\ 4/3 & \left(^3\mathrm{P}_0\right)\end{cases} \tag{26}$$

Thus in the Klempt model, we get a clear indication that the large value of $\gamma_1(^3\mathrm{P}_1)/\gamma_0(^3\mathrm{P}_1)$ (6.7 in Table 2) expected theoretically, and arising because of the repulsive tensor potential in the $^{13}\mathrm{P}_1$ channel, is indeed seen in the data. In the $^3\mathrm{P}_0$ model, on the other hand, the factor ξ is smaller, and the restriction (26) is much weaker. The other dramatic prediction

of the isospin mixing calculations, namely that $\gamma_0(^3P_0) \gg \gamma_1(^3P_0)$, is difficult to confirm based on the existing data. The problem is that there are no transitions which are fed *only* by the $^3P_0$ channel; in all cases, the $^3P_2$ or $^3P_1$ (or both) initial states also contribute, and the branching ratio $N\bar{N}(^3P_J) \rightarrow M_1M_2$ is not very sensitive to the $^3P_0$ part, which has the lowest statistical weight $(2J+1)$.

7. Conclusions

The problem of initial and final state interactions in $N\bar{N}$ annihilation is a very complicated one. It is clear from various estimates that such interactions strongly distort predictions for relative branching ratios based on the Born approximation. What is not clear is how to incorporate these interactions in a quantitative way. In the present paper, we compare two models in which the effect of initial state interactions in the $N\bar{N}$ atom is expressed in terms of probabilities γ_I^i that states $i = \{LSJ\}$ have isospin components $I = 0, 1$. These γ_I^i depend very strongly on i, particularly for $L = 1$ initial states. The dominant effect at work here is the $I = 0$ tensor force, which is coherently attractive for $L = J \pm 1$ and repulsive for $L = J$. We have investigated the sensitivity of γ_I^i to modifications of the vector meson contribution to the tensor potential. Our conclusion is that the dramatic effects of short range $p\bar{p} - n\bar{n}$ mixing already occur when only single pion exchange is included, and that there is no qualitative modification of γ_I^i from (ρ, ω) exchange.

The two models that we study, in addition to γ_I^i, incorporate a channel dependent spin–flavor factor. In the first model, due to Klempt[17], this factor is assumed to depend only on isospins, whereas in the second model, we use the $^3P_0$ spin–flavor recoupling factors. Both of these models can be adjusted to produce a number of relative branching ratios for $L = 0$. However, they give dramatically different predictions for certain transitions from initial $L = 1$ $N\bar{N}$ states. Data which will become available from experiments at the LEAR facility at CERN should clearly distinguish between the two models considered here, enabling us to reject one, or more likely both, of them.

We have identified some problems with both the Klempt[17] and $^3P_0$ models, based on the existing data. Note that we have considered only one form of the $^3P_0$ model, with the planar

$A2$ topology of Fig. 3. Some admixture of rearrangement amplitudes[9] may improve the situation. However, there are a number of conceptual problems with such simple models. The use of isospin probabilities γ_I^i clearly does not take into account the interferences which are likely to be strong for tensor–coupled partial waves, particularly $^{13}S_1$–$^{13}D_1$ and $^{13}P_2$–$^{13}F_2$. Maruyama *et al.*[10] have shown that $^{13}S_1$–$^{13}D_1$ constructive interference is very important for an understanding of the "$\pi\rho$ puzzle". There is another potentially serious problem with the use of probabilities. These result from an *average* over the annihilation region, in the context of an optical model calculation of $N\overline{N}$ wave functions. Inspection of these wave functions reveals that the $I = 1$ to $I = 0$ ratio depends sensitively on the distance r. When one isospin component dominates, the effect is most pronounced at short distances, in the region which is relevant for the sizable q values characteristic of two–body final states. Thus, the branching ratios may not reflect the average values γ_I^i. Further, our estimates of γ_I^i have been obtained by assuming a local and channel independent annihilation potential $W(r)$. In microscopic models, W is non–local and spin–isospin dependent, so our assumption is clearly an oversimplification. Nevertheless, we still find it useful to investigate simple treatments of initial state interactions, in order to see where they break down. This may provide some hints as to how to proceed to a more refined picture of the low energy $N\overline{N}$ annihilation process.

Acknowledgments

It is a pleasure to thank E. Klempt for several useful discussions on antinucleon annihilation. J.M.R. benefitted from the hospitality provided by the Nuclear Theory Group at Broookhaven and by the Physics Division at CEBAF, during visits to these institutions. The work of C.B.D. was supported by the U.S. Department of Energy under contract No. DE–AC02–76CH00016.

REFERENCES

1. I.S. Shapiro, Phys. Rep. C35, 129 (1978).
2. W.W. Buck, C.B. Dover and J.M. Richard, Ann. Phys. (NY) 121, 47 (1979).
3. C.B. Dover and J.M. Richard, Phys. Rev. D17, 1770 (1978).
4. W.B. Kaufmann and H. Pilkuhn, Phys. Rev. C17, 215 (1978).
5. W.B. Kaufmann, Phys. Rev. C19, 440 (1979).
6. J.M. Richard and M.E. Sainio, Phys. Lett. 110B, 349 (1982).
7. J. Carbonell, G. Ihle and J.-M. Richard, Z. Phys. A334, 329 (1989).
8. C.B. Dover, in *Intersections between Particle and Nuclear Physics*, Rockport, Maine; AIP Conf. Proc. 176, Ed. G.M. Bunce, AIP, New York, 1988, p. 370.
9. M. Maruyama, S. Furui and A. Faessler, Nucl. Phys. A472, 643 (1987).
10. M. Maruyama, T. Gutsche, G. Strobel, A. Faessler and E. Henley, Phys. Lett. 215B, 223 (1988).
11. S. Mundigl, M. Vicente Vacas and W. Weise, Z. Phys. A338, 103 (1991).
12. C.B. Dover and J.-M. Richard, Phys. Rev. C21, 1466 (1980).
13. M. Kohno and W. Weise, Nucl. Phys. A454, 429 (1986).
14. S. Furui, G. Strobel, A. Faessler and R. Vinh Mau, Nucl. Phys. A516, 643 (1990).
15. C.A. Amsler, Nucl. Phys. A508, 501c (1990).
16. C.B. Dover, J.M. Richard and M. Zabek, Ann. Phys. (NY) 130, 70 (1980).
17. E. Klempt, Phys. Lett. B244, 122 (1990); B245, 129 (1990).
18. N.A. Roe *et al.*, Phys. Rev. D41, 17 (1990);
    H. Aihara *et al.*, Phys. Rev. Lett. 64, 172 (1990).
19. Note that we write the statistical factor as $2J+1$ rather than $2S+1$, as Klempt[17] does. For $L=0$, they are of course the same. In addition, we insert a factor $\Gamma_{\rm tot}^{-1}$ in Eq. (3), to account for the differing total annihilation widths of the states i. Klempt omits this factor, which is equivalent to assuming that all widths are the same. This is reasonable for $L=0$, since $\Gamma(^1{\rm S}_0) \approx \Gamma(^3{\rm S}_1)$; we adopt this approximation here for $L=0$. For $L=1$, the widths for $^1{\rm P}_1$ and $^3{\rm P}_J$ are quite different (see Table 2).

20. Note that for tensor coupled states such as $^{13}S_1$–$^{13}D_1$, $^{13}P_2$–$^{13}F_2$, etc., L is not a good quantum number. Our calculations include the full effects of tensor as well as $p\bar{p} - n\bar{n}$ coupling.

21. We give slightly different values for the ratios of $C(I; I_1 I_2)$ factors than found in Ref. 17.

22. J. Vandermeulen, Z. Phys. C37, 563 (1988).

23. C.B. Dover and P. Fishbane, Nucl. Phys. B244, 349 (1984);
C.B. Dover, P. Fishbane and S. Furui, Phys. Rev. Lett. 57, 1538 (1986).

24. R. Bizzarri *et al.*, Nucl. Phys. B14, 169 (1969).

25. C. Baltay *et al.*, Phys. Rev. 140, B1042 (1965).

26. M. Bloch *et al.*, Nucl. Phys. B23, 221 (1970).

27. J. Diaz *et al.*, Nucl. Phys. B16, 239 (1970).

28. C. Baltay *et al.*, Phys. Rev. 145, 1103 (1966).

29. B. May *et al.*, Z. Phys. C46, 203 (1990).

Table Captions

Table 1: Real part of energy shift ΔE, total width $\Gamma = \Gamma_0 + \Gamma_1$ and ratio $y = \Gamma_1/\Gamma_0$ of annihilation widths in $I = 1$ and $I = 0$ states for the $^1S_0$, $^1P_1$, $^3P_0$ and $^3P_1$ levels of protonium, as calculated from the optical model of Dover and Richard (DR2), with variable strength x of the $2\pi + \omega$ exchange potential. Units of ΔE and Γ are keV for S–states and meV for P–states.

Table 2: Isospin probabilities γ_I^i for $L = 0, 1$ atomic $N\overline{N}$ states[a,b,c].

Table 3: Ratios of branching rates for $L = 0$ $N\overline{N}$ annihilation at rest[a,b,c].

Table 4: Predicted ratios of branching ratios B for neutral modes in $N\overline{N}$ $(L = 1) \rightarrow$ $M_1 M_2$ annihilation.

Table 5: Predicted ratios of charged to neutral modes for $N\overline{N}$ $(L = 1)$ annihilations.

Table 1

	$^1S_0$			$^1P_1$			$^3P_0$			$^3P_1$		
x	ΔE	Γ	y	ΔE	Γ	y	ΔE	Γ	y	ΔE	Γ	y
1.0	0.58	0.52	0.80	-24	14	0.61	-62	40	0.053	36	8.8	6.5
0.8	0.57	0.50	0.73	-23	14	0.62	-57	45	0.045	37	8.7	6.8
0.6	0.56	0.48	0.66	-22	15	0.65	-55	54	0.038	38	8.8	7.2
0.4	0.56	0.47	0.59	-22	15	0.67	-60	63	0.033	39	9.1	7.8
0.2	0.56	0.45	0.55	-22	15	0.64	-72	67	0.032	39	9.5	8.4
0.0	0.56	0.44	0.51	-22	14	0.58	-83	61	0.037	39	9.8	9.0

Table 2

State i	$\gamma_0(i)$	$\gamma_1(i)$	$\Gamma_{\rm tot}(i)$
$^1S_0$	0.56	0.44	1.0
$^3S_1$–$^3D_1$	0.56	0.44	0.9
$^1P_1$	0.62	0.38	28.6
$^3P_0$	0.95	0.05	80.0
$^3P_1$	0.13	0.87	17.6
$^3P_2$–$^3F_2$	0.60	0.40	32.8

a. We use the values for model DR2, with $x = 1$, and tensor coupling included.

b. For $\gamma_I(^1S_0)$ and $\gamma_I(^3S_1 - {}^3D_1)$, we use the notation γ_I^s and γ_I^t, respectively, in the text.

c. $\Gamma_{\rm tot}$ in keV for $L = 0$, in meV for $L = 1$.

Table 3

Ratio	Klempt Model (Eq. (3))	$^3P_0$ Model (Eq. (6))
$B^s(\rho^0\rho^0)/B^s(\omega\omega)$	$\frac{C(0;11)}{C(0;00)}$ [3/4]	1
$B^s(\rho^0\omega)/B^s(\omega\omega)$	$\frac{\gamma_1^s C(1;01)}{\gamma_0^s C(0;00)}$ [0.4]	$\frac{50\gamma_1^s}{9\gamma_0^s}$ [4.4]
$B^s(\pi^0 a_2^0)/B^s(\pi^0 f_2)$	$\frac{\gamma_0^s C(0;11)}{\gamma_1^s C(1;01)}$ [1.9]	$\frac{9\gamma_0^s}{25\gamma_1^s}$ [0.5]
$B^t(\pi^0 b_1^0)/B^t(\pi^0 h_1)$	$\frac{\gamma_0^t C(0;11)}{\gamma_1^t C(1;01)}$ [1.9]	$\frac{4\gamma_0^t}{3\gamma_1^t}$ [1.7]

a. We use the standard notation $a_2 = a_2(1320)[J^{\pi C}(I^G) = 2^{++}(1^-)]$, $b_1 = b_1(1235)[1^{+-}(1^+)]$, $f_2 = f_2(1270)[2^{++}(0^+)]$.

b. As in the text, the notation $B^s(\rho^0\rho^0)$ stands for $B(^{11}S_0 \to \rho^0\rho^0(\ell = 1))$, etc. For $\pi^0 b_1^0$ and $\pi^0 h_1$, both $\ell = 0$ and $\ell = 2$ are possible, and the ratio is the same for each in both models.

c. The numbers in brackets are obtained using Eqs. (4a–4c) and Table 2.

Table 4

Ratio	Klempt Model (Eq. (3))	$^3P_0$ Model (Eq. (6))
$\frac{B(^3P_{0,2}\to\rho^0\rho^0(\ell=0,2))}{B(^3P_{0,2}\to\omega\omega(\ell=0,2))}$	0.8	1
$\frac{B(^3P_{0,1,2}\to\rho^0\omega(\ell=0,2))}{B(^3P_{0,2}\to\omega\omega(\ell=0,2))}$	1.0	0.7 ($\ell=0$), 3.2 ($\ell=2$)
$\frac{B(^3P_{1,2}\to\pi^0 a_2^0(\ell=1))}{B(^3P_{1,2}\to\pi^0 f_2(\ell=1))}$	0.8	0.3
$\frac{B(^1P_1\to\pi^0 b_1^0(\ell=1))}{B(^1P_1\to\pi^0 h_1(\ell=1))}$	2.5	both zero!

Table 5

Ratio	Klempt Model (Eq. (3))	$^3P_0$ Model (Eq. (6))
$\frac{B(^3P_1 \to \pi^+\rho^-(\ell=0))}{B(^1P_1 \to \pi^0\rho^0(\ell=0))}$	0.3	6.3
$\frac{B(^3P_{1,2} \to \pi^+\rho^-(\ell=2))}{B(^1P_1 \to \pi^0\rho^0(\ell=2))}$	0.4	3.9
$\frac{B(^1P_1 \to \rho^+\rho^-(\ell=0))}{B(^3P_{0,2} \to \rho^0\rho^0(\ell=0))}$	0.05	0.17
$\frac{B(^1P_1 \to \rho^+\rho^-(\ell=2))}{B(^3P_{0,2} \to \rho^0\rho^0(\ell=2))}$	0.05	0.25
$\frac{B(^1P_1 \to \pi^+a_1^-(\ell=1))}{B(^3P_{0,1,2} \to \pi^0a_1^0(\ell=1))}$	0.04	0.07
$\frac{B(^1P_1 \to \pi^+a_2^-(\ell=1))}{B(^3P_{1,2} \to \pi^0a_2^0(\ell=1))}$	0.05	0.8

Figure Captions

Fig. 1: Annihilation density $d(r)$ for the $I = 0$ component of the $^3P_0$ state of protonium, with the full meson exchange potential ($x = 1$) or with the pion tail only ($x = 0$). Units are fm for the distance r and meV/fm for the density.

Fig. 2: Same as Fig. 1, but for the $I = 1$ component.

Fig. 3: Planar annihilation diagram "A2" describing nucleon–antinucleon annihilation into two mesons.

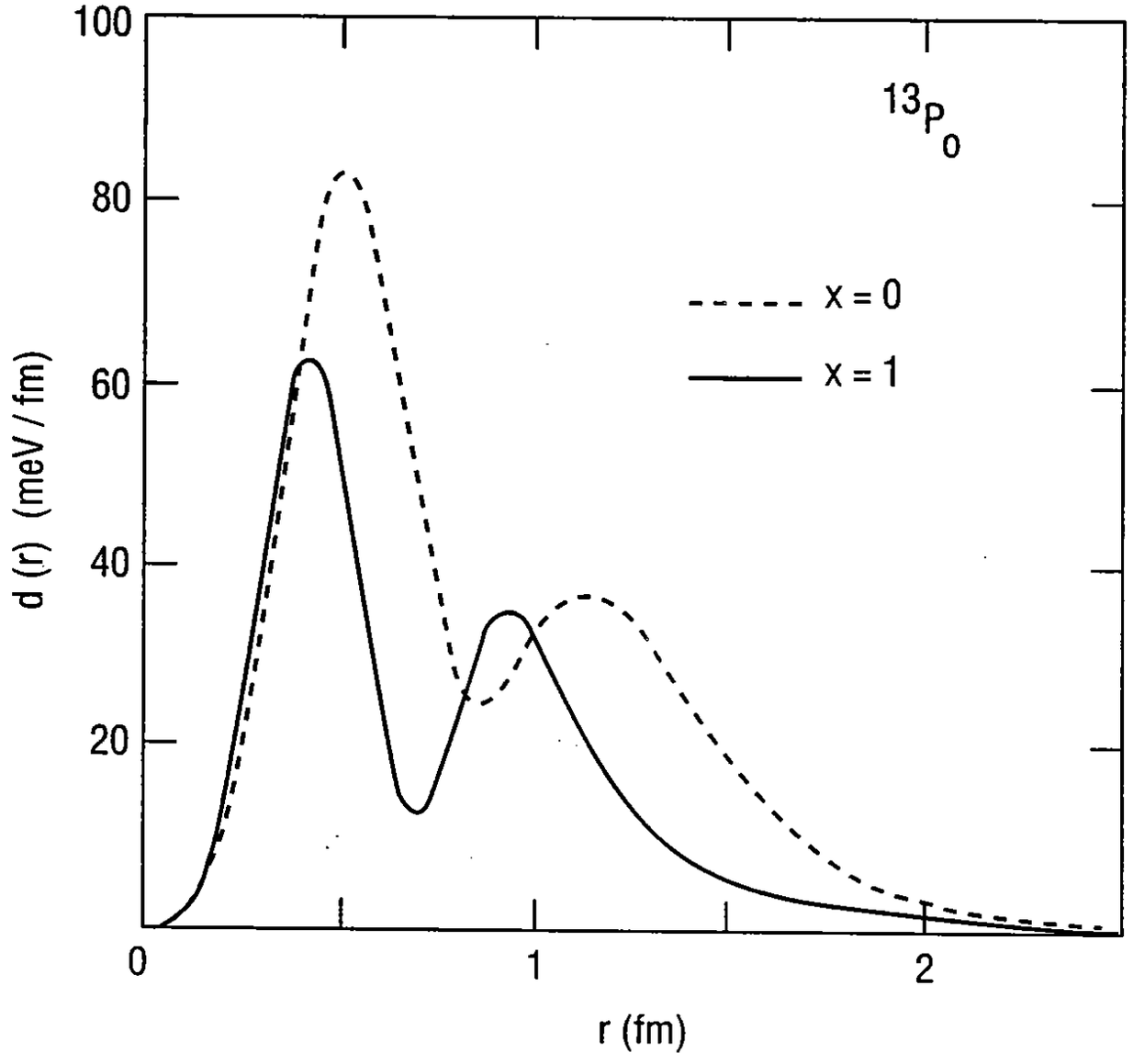

FIG. 1

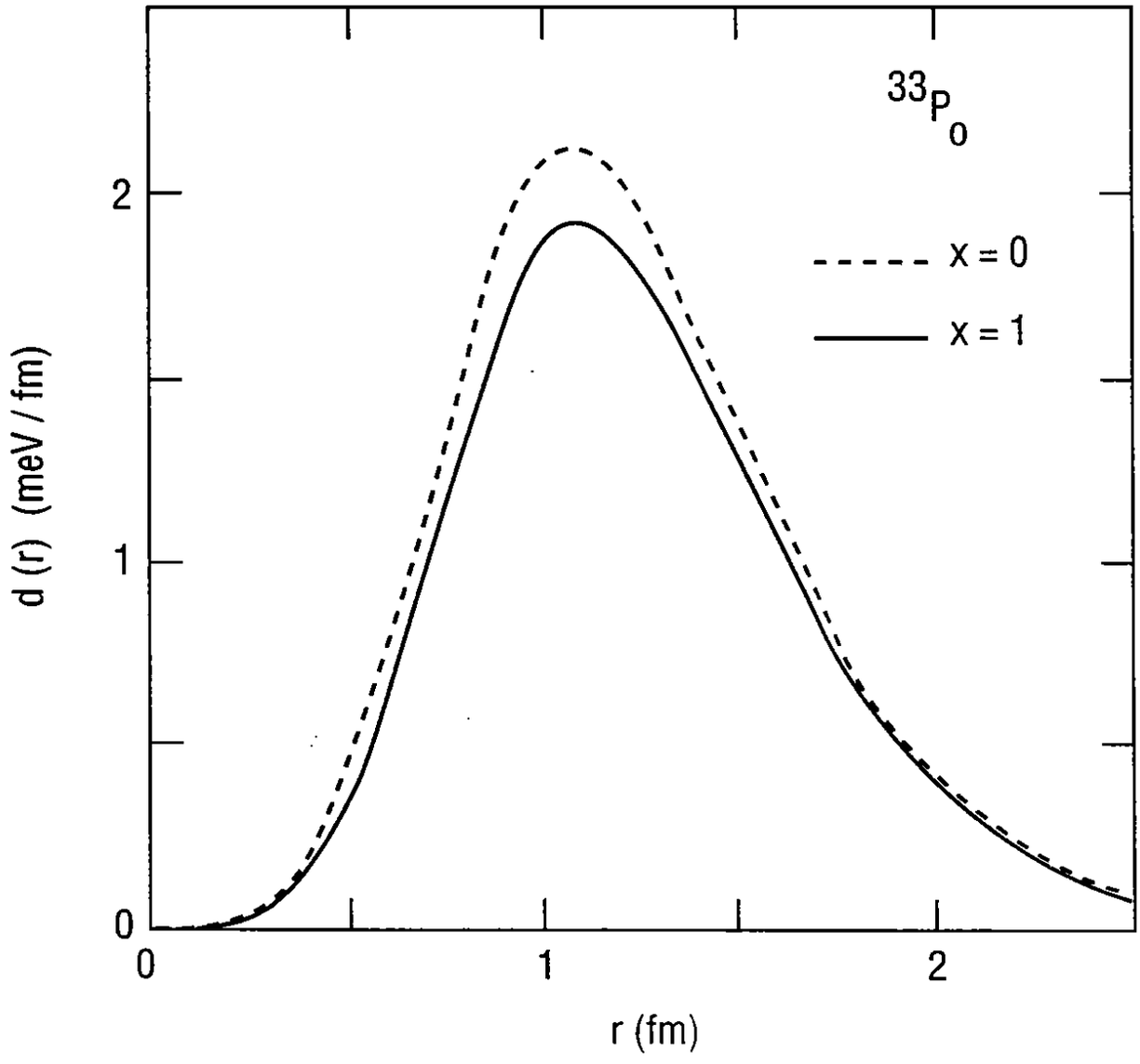

FIG. 2

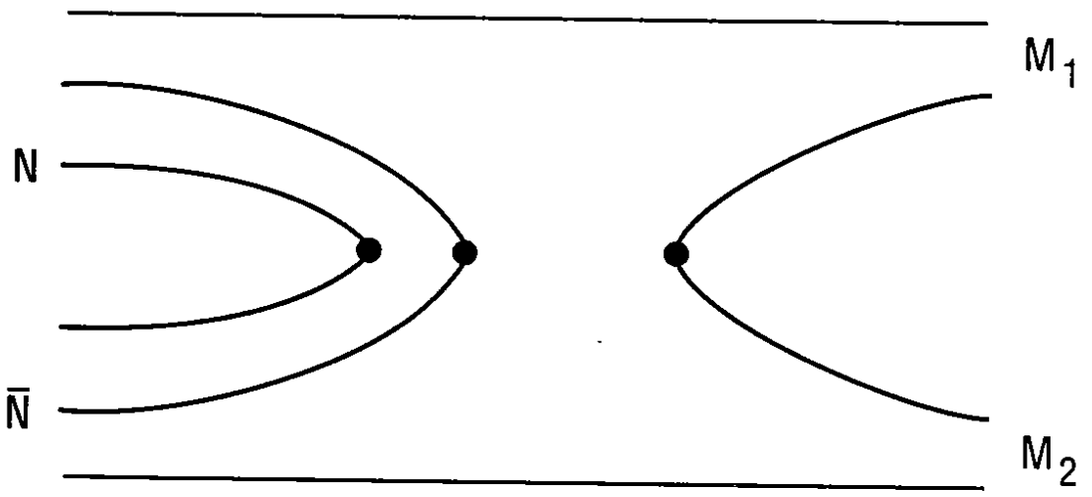

FIG. 3